

$\Lambda_b \rightarrow p \ell^- \bar{\nu}_\ell$ form factors from lattice QCD with static b quarks

William Detmold,¹ C.-J. David Lin,² Stefan Meinel,^{1,*} and Matthew Wingate³

¹*Center for Theoretical Physics, Massachusetts Institute of Technology, Cambridge, MA 02139, USA*

²*Institute of Physics, National Chiao-Tung University, Hsinchu 300, Taiwan*

³*DAMTP, University of Cambridge, Wilberforce Road, Cambridge CB3 0WA, UK*

(Dated: June 3, 2013)

We present a lattice QCD calculation of form factors for the decay $\Lambda_b \rightarrow p \mu^- \bar{\nu}_\mu$, which is a promising channel for determining the CKM matrix element $|V_{ub}|$ at the Large Hadron Collider. In this initial study we work in the limit of static b quarks, where the number of independent form factors reduces to two. We use dynamical domain-wall fermions for the light quarks, and perform the calculation at two different lattice spacings and at multiple values of the light-quark masses in a single large volume. Using our form factor results, we calculate the $\Lambda_b \rightarrow p \mu^- \bar{\nu}_\mu$ differential decay rate in the range $14 \text{ GeV}^2 \leq q^2 \leq q_{\text{max}}^2$, and obtain the integral $\int_{14 \text{ GeV}^2}^{q_{\text{max}}^2} [d\Gamma/dq^2] dq^2 / |V_{ub}|^2 = 15.3 \pm 4.2 \text{ ps}^{-1}$. Combined with future experimental data, this will give a novel determination of $|V_{ub}|$ with about 15% theoretical uncertainty. The uncertainty is dominated by the use of the static approximation for the b quark, and can be reduced further by performing the lattice calculation with a more sophisticated heavy-quark action.

PACS numbers: 12.15.Ff, 12.38.Gc, 13.30.Ce, 14.20.Mr

I. INTRODUCTION

A long-standing puzzle in flavor physics is the discrepancy between the extractions of the CKM matrix element $|V_{ub}|$ from inclusive and exclusive B meson semileptonic decays at the B factories [1–4]. The current average values determined by the Particle Data Group are [4]

$$|V_{ub}|_{\text{incl.}} = (4.41 \pm 0.15_{-0.17}^{+0.15}) \cdot 10^{-3}, \quad (1)$$

$$|V_{ub}|_{\text{excl.}} = (3.23 \pm 0.31) \cdot 10^{-3}, \quad (2)$$

where the exclusive determination is based on measurements of $\bar{B} \rightarrow \pi^+ \ell^- \bar{\nu}_\ell$ decays by the BABAR and BELLE collaborations, and uses $\bar{B} \rightarrow \pi^+$ form factors computed in lattice QCD [5, 6]. To address the discrepancy between Eqs. (1) and (2), new and independent determinations of $|V_{ub}|$ are desirable. At the Large Hadron Collider, measurements of $\bar{B} \rightarrow \pi^+ \ell^- \bar{\nu}_\ell$ branching fractions are difficult because of the large pion background; therefore an attractive possibility is to use instead the baryonic mode $\Lambda_b \rightarrow p \ell^- \bar{\nu}_\ell$, which has a more distinctive final state [7]. In order to determine $|V_{ub}|$ from this measurement, the $\Lambda_b \rightarrow p$ form factors need to be calculated in nonperturbative QCD.

The $\Lambda_b \rightarrow p$ matrix elements of the vector and axial vector $b \rightarrow u$ currents are parametrized in terms of six independent form factors (see, e.g., Ref. [8]). In leading-order heavy-quark effective theory (HQET), which becomes exact in the limit $m_b \rightarrow \infty$ and is a good approximation at the physical value of m_b , only two independent form factors remain, and the matrix element with arbitrary Dirac matrix Γ in the current can be written as [8–10]

$$\langle N^+(p', s') | \bar{u} \Gamma Q | \Lambda_Q(v, s) \rangle = \bar{u}_N(p', s') [F_1 + \not{v} F_2] \Gamma u_{\Lambda_Q}(v, s). \quad (3)$$

Above, v is the four-velocity of the Λ_Q baryon, and the form factors F_1, F_2 are functions of $p' \cdot v$, the energy of the proton in the Λ_Q rest frame (we denote the heavy quark defined in HQET by Q , and we denote the proton by N^+). Note that in leading-order soft-collinear effective theory, which applies in the limit of large $p' \cdot v$, the form factor F_2 vanishes [11–13].

Calculations of $\Lambda_b \rightarrow p$ form factors have been performed using QCD sum rules [14, 15] and light-cone sum rules [16–19]. Light-cone sum rules are most reliable at low q^2 (corresponding to large proton momentum in the Λ_b rest frame), and even there the uncertainty of the best available calculations is of order 20% [19]. As we will see later, the $\Lambda_b \rightarrow p \ell^- \bar{\nu}_\ell$ differential decay rate has its largest value in the high- q^2 (low hadronic recoil) region. This is also the region where lattice QCD calculations can be performed with the highest precision.

* smeinel@mit.edu

Lattice QCD determinations of the form factors for the mesonic decay $\bar{B} \rightarrow \pi^+ \ell^- \bar{\nu}_\ell$ are already available [5, 6], and several groups are working on new calculations [20–22]. We have recently published the first lattice QCD calculation of $\Lambda_Q \rightarrow \Lambda$ form factors, which are important for the rare decay $\Lambda_b \rightarrow \Lambda \ell^+ \ell^-$ [23]. We performed this calculation at leading order in HQET, i.e., with static heavy quarks. The HQET form factors F_1 and F_2 for the $\Lambda_Q \rightarrow \Lambda$ transition are defined as in Eq. (3), except that the current is $\bar{s}\Gamma Q$ and the final state is the Λ baryon. In the following, we report the first lattice QCD determination of the $\Lambda_Q \rightarrow p$ form factors defined in Eq. (3), building upon the analysis techniques developed in Ref. [23]. The calculation uses dynamical domain wall fermions [24–26] for the up-, down-, and strange quarks, and is based on gauge field ensembles generated by the RBC/UKQCD collaboration [27].

In Sec. II, we outline our extraction of the $\Lambda_Q \rightarrow p$ form factors from ratios of correlation functions, and present the lattice parameters and form factor results for each data set. In Sec. III, we present our fits of the lattice-spacing-, quark-mass-, and $(p' \cdot v)$ -dependence of these results, and discuss systematic uncertainties. We compare the $\Lambda_Q \rightarrow p$ form factors computed here to previous determinations of both $\Lambda_Q \rightarrow p$ and $\Lambda_Q \rightarrow \Lambda$ form factors in Sec. IV. Using our form factor results, we then calculate the differential decay rates of $\Lambda_b \rightarrow p \ell^- \bar{\nu}_\ell$ for $\ell = e, \mu, \tau$ in Sec. V. Finally, in Sec. VI we discuss the impact of our results on future determinations of $|V_{ub}|$ from these decays, and the prospects for more precise lattice calculations.

II. LATTICE CALCULATION

We performed the calculation of the $\Lambda_Q \rightarrow p$ form factors with the same lattice actions and parameters as used in our calculation of the $\Lambda_Q \rightarrow \Lambda$ form factors in Ref. [23]. That is, we are using a domain-wall action for the up, down, and strange quarks [24–26], the Iwasaki action [28, 29] for the gluons, and the Eichten-Hill action [30] with HYP-smearing gauge links [31] for the static heavy quark. The Eichten-Hill action requires that we work in the Λ_Q rest frame, i.e. with $v = (1, 0, 0, 0)$. We compute “forward” and “backward” three-point functions

$$C_{\delta\alpha}^{(3)}(\Gamma, \mathbf{p}', t, t') = \sum_{\mathbf{y}} e^{-i\mathbf{p}' \cdot (\mathbf{x} - \mathbf{y})} \langle N_\delta(x_0, \mathbf{x}) J_\Gamma^\dagger(x_0 - t + t', \mathbf{y}) \bar{\Lambda}_{Q\alpha}(x_0 - t, \mathbf{y}) \rangle, \quad (4)$$

$$C_{\alpha\delta}^{(3,bw)}(\Gamma, \mathbf{p}', t, t - t') = \sum_{\mathbf{y}} e^{-i\mathbf{p}' \cdot (\mathbf{y} - \mathbf{x})} \langle \Lambda_{Q\alpha}(x_0 + t, \mathbf{y}) J_\Gamma(x_0 + t', \mathbf{y}) \bar{N}_\delta(x_0, \mathbf{x}) \rangle, \quad (5)$$

containing the baryon interpolating fields

$$\Lambda_{Q\alpha} = \epsilon^{abc} (C\gamma_5)_{\beta\gamma} \tilde{d}_\beta^a \tilde{u}_\gamma^b Q_\alpha^c, \quad (6)$$

$$N_\alpha = \epsilon^{abc} (C\gamma_5)_{\beta\gamma} \tilde{u}_\beta^a \tilde{d}_\gamma^b \tilde{u}_\alpha^c, \quad (7)$$

and the current

$$J_\Gamma = U(m_b, a^{-1}) \mathcal{Z} \left[\left(1 + c_\Gamma^{(ma)} \frac{m_u a}{1 - (w_0^{\text{MF}})^2} \right) \bar{Q}\Gamma u + c_\Gamma^{(pa)} a \bar{Q}\Gamma \gamma \cdot \nabla u \right]. \quad (8)$$

In the baryon interpolating fields, the tilde on the up- and down-quark fields indicates Gaussian gauge-covariant smearing. The coefficients \mathcal{Z} , $c_\Gamma^{(ma)}$, and $c_\Gamma^{(pa)}$ in the current (8) provide an $\mathcal{O}(a)$ -improved matching from lattice HQET to continuum HQET in the $\overline{\text{MS}}$ scheme; they have been computed in one-loop perturbation theory in Ref. [32]. The factor $U(m_b, a^{-1})$ provides two-loop renormalization-group running in continuum HQET from the scale $\mu = a^{-1}$ (where a is the lattice spacing) to the desired scale $\mu = m_b$.

Note that, because Eq. (7) contains two up-quark fields, the $\Lambda_Q \rightarrow p$ three-point functions contain two different types of contractions of quark propagators, one of which is not present in the $\Lambda_Q \rightarrow \Lambda$ three-point functions studied in Ref. [23]. This is also the case for the proton two-point functions.

We multiply the forward- and backward three-point functions and form the ratio [23]

$$\mathcal{R}(\Gamma, \mathbf{p}', t, t') = \frac{4 \text{Tr} [C^{(3)}(\Gamma, \mathbf{p}', t, t') C^{(3,bw)}(\Gamma, \mathbf{p}', t, t - t')]}{\text{Tr}[C^{(2,N)}(\mathbf{p}', t)] \text{Tr}[C^{(2,\Lambda_Q)}(t)]}, \quad (9)$$

where $C^{(2,N)}(\mathbf{p}', t)$ and $C^{(2,\Lambda_Q)}(t)$ are the proton and the Λ_Q two-point functions, and the traces are over spinor indices. The ratio is computed using the statistical bootstrap method. As explained in Ref. [23], we then form the combinations

$$\mathcal{R}_+(\mathbf{p}', t, t') = \frac{1}{4} [\mathcal{R}(1, \mathbf{p}', t, t') + \mathcal{R}(\gamma^2 \gamma^3, \mathbf{p}', t, t') + \mathcal{R}(\gamma^3 \gamma^1, \mathbf{p}', t, t') + \mathcal{R}(\gamma^1 \gamma^2, \mathbf{p}', t, t')], \quad (10)$$

$$\mathcal{R}_-(\mathbf{p}', t, t') = \frac{1}{4} [\mathcal{R}(\gamma^1, \mathbf{p}', t, t') + \mathcal{R}(\gamma^2, \mathbf{p}', t, t') + \mathcal{R}(\gamma^3, \mathbf{p}', t, t') + \mathcal{R}(\gamma_5, \mathbf{p}', t, t')], \quad (11)$$

which, upon inserting Eq. (3) into the transfer matrix formalism, yield

$$\mathcal{R}_+(\mathbf{p}', t, t') = \frac{E_N + m_N}{E_N} [F_1 + F_2]^2 + \dots, \quad (12)$$

$$\mathcal{R}_-(\mathbf{p}', t, t') = \frac{E_N - m_N}{E_N} [F_1 - F_2]^2 + \dots \quad (13)$$

Here, the ellipses denote excited-state contributions that decay exponentially with the Euclidean time separations, and F_1, F_2 are the form factors at the given values of the proton momentum \mathbf{p}' , the lattice spacing, and the quark masses. Throughout the remainder of this paper, we will use the following names for the combinations of form factors that appear in Eqs. (12), (13):

$$F_+ = F_1 + F_2, \quad F_- = F_1 - F_2. \quad (14)$$

For a given value of $|\mathbf{p}'|^2$, we further average Eqs. (10) and (11) over the direction of \mathbf{p}' , and we denote the resulting quantities as $\mathcal{R}_\pm(|\mathbf{p}'|^2, t, t')$. As a consequence of the symmetric form of the ratio (9), at a given source-sink separation t , the contamination from excited states is smallest at the mid-point $t' = t/2$. We therefore construct the following functions

$$R_+(|\mathbf{p}'|^2, t) = \sqrt{\frac{E_N}{E_N + m_N} \mathcal{R}_+(|\mathbf{p}'|^2, t, t/2)}, \quad (15)$$

$$R_- (|\mathbf{p}'|^2, t) = \sqrt{\frac{E_N}{E_N - m_N} \mathcal{R}_-(|\mathbf{p}'|^2, t, t/2)}, \quad (16)$$

which, according to Eqs. (12), (13), become equal to the form factors F_+ and F_- for large source-sink separation, t .

We performed the numerical calculations for the six different sets of parameters shown in Table I. When evaluating Eqs. (15) and (16), we used the lattice results for the proton mass, m_N , obtained from fits to the proton two-point function in the same data set. These results are also given in Table I. Unlike in Ref. [23], here we calculated the energies at nonzero momentum using the relativistic continuum dispersion relation $E_N = \sqrt{m_N^2 + |\mathbf{p}'|^2}$. The energies calculated in this way are consistent with the energies obtained directly from fits to the proton two-point functions at nonzero momentum, but using the relativistic dispersion relation reduces the uncertainty. We computed $R_\pm(|\mathbf{p}'|^2, t)$ for proton momenta in the range $0 \leq |\mathbf{p}'|^2 \leq 9 \cdot (2\pi/L)^2$, where $L = N_s a \approx 2.7$ fm is the spatial size of the lattice. We performed the calculation for all source-sink separations from $t/a = 4$ to $t/a = 15$ at the coarse lattice spacing (data sets C14, C24, C54), and for $t/a = 5$ to $t/a = 20$ at the fine lattice spacing (data sets F23, F43, F63). This wide range of source-sink separations allows us to reliably extract the ground-state form factors [23]. Because the statistical uncertainties grow exponentially with t , in practice the upper limit of t/a we can use is somewhat smaller, especially at larger momentum.

A plot of example numerical results for $R_\pm(|\mathbf{p}'|^2, t)$ as a function of the source-sink separation t is shown in Fig. 1. The results are qualitatively similar to those obtained for the Λ final state in Ref. [23] (the t' -dependence of $\mathcal{R}_\pm(|\mathbf{p}'|^2, t, t')$ is also similar to that seen in Ref. [23]). It can be seen that there is contamination from excited states which decays exponentially with t . At $|\mathbf{p}'|^2 \neq 0$ we perform fits of the t -dependence using the functions

$$R_\pm^{i,n}(t) = F_\pm^{i,n} + A_\pm^{i,n} \exp[-\delta^{i,n} t], \quad (17)$$

which account for the leading excited-state contamination [23]. Above, we use an abbreviated notation where n specifies the squared momentum of the proton [we write $|\mathbf{p}'|^2 = n \cdot (2\pi/L)^2$], and $i = \text{C14, C24, ..., F63}$ specifies the data set. To enforce the positivity of the energy gaps $\delta^{i,n}$, we rewrite them as $\delta^{i,n}/(1 \text{ GeV}) = \exp(l^{i,n})$. The fit parameters in Eq. (17) are then $F_\pm^{i,n}$, $A_\pm^{i,n}$, and $l^{i,n}$. Note that we perform coupled fits of $R_+^{i,n}$ and $R_-^{i,n}$ with common energy gap parameters, which improves the statistical precision of the fits [23]. As a check, we have also performed independent fits with separate energy gap parameters $l_+^{i,n}$ and $l_-^{i,n}$ and found that $l_+^{i,n}$ and $l_-^{i,n}$ are in agreement within statistical uncertainties.

At a given momentum-squared n , we perform the fits using Eq. (17) simultaneously for the six different data sets $i = \text{C14, C24, ..., F63}$. Because the lattice size, L (in physical units), is equal within uncertainties for all data sets, the squared momentum $|\mathbf{p}'|^2 = n \cdot (2\pi/L)^2$ for a given n is also equal within uncertainties for all data sets. To improve the stability of the fits, we augment the χ^2 function by adding a term that limits the variation of $l^{i,n}$ across the data sets to reasonable values [23].

At $\mathbf{p}' = 0$, we can only compute $R_+^{i,0}(t)$, and we find that the t -dependence of $R_+^{i,0}(t)$ is weak. In this case we are unable to perform exponential fits, and we instead perform constant fits, excluding a few points at the shortest t .

The numerical results for the form factors $F_\pm^{i,n}$ are listed in Tables II and III. The uncertainties shown there are the quadratic combination of the statistical uncertainty and an estimate of the systematic uncertainty associated

Set	β	$N_s^3 \times N_t \times N_5$	am_5	$am_s^{(\text{sea})}$	$am_{u,d}^{(\text{sea})}$	a (fm)	$am_{u,d}^{(\text{val})}$	$m_\pi^{(\text{val})}$ (MeV)	$m_N^{(\text{val})}$ (MeV)	N_{meas}
C14	2.13	$24^3 \times 64 \times 16$	1.8	0.04	0.005	0.1119(17)	0.001	245(4)	1090(21)	2672
C24	2.13	$24^3 \times 64 \times 16$	1.8	0.04	0.005	0.1119(17)	0.002	270(4)	1103(20)	2676
C54	2.13	$24^3 \times 64 \times 16$	1.8	0.04	0.005	0.1119(17)	0.005	336(5)	1160(19)	2782
F23	2.25	$32^3 \times 64 \times 16$	1.8	0.03	0.004	0.0849(12)	0.002	227(3)	1049(25)	1907
F43	2.25	$32^3 \times 64 \times 16$	1.8	0.03	0.004	0.0849(12)	0.004	295(4)	1094(18)	1917
F63	2.25	$32^3 \times 64 \times 16$	1.8	0.03	0.006	0.0848(17)	0.006	352(7)	1165(23)	2782

TABLE I. Lattice parameters. The data sets C14, C24 and C54 all correspond to the same “coarse” ensemble of gauge fields with gauge coupling $\beta = 6/g^2 = 2.13$ and sea-quark masses $am_s^{(\text{sea})} = 0.04$, $am_{u,d}^{(\text{sea})} = 0.005$; these data sets differ only in the values of the valence-quark mass, $am_{u,d}^{(\text{val})}$, used for the domain wall propagators. At the “fine” lattice spacing, the propagators in the F23 and F43 data sets are from one common ensemble of gauge fields, but the F63 data set is obtained from a different ensemble with heavier sea-quark masses. In each case, we also list the valence pion and proton masses, $m_\pi^{(\text{val})}$ and $m_N^{(\text{val})}$, and the number of light-quark propagators, N_{meas} , used for our analysis. The ensembles of gauge fields have been generated by the RBC/UKQCD collaboration; see Ref. [27] for further details.

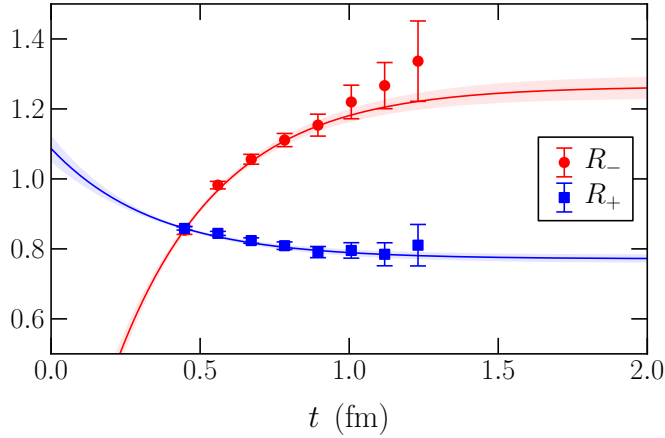


FIG. 1. Example of numerical results for $R_\pm(|\mathbf{p}'|^2, t)$, plotted as a function of the source-sink separation t , along with a fit using Eq. (17). The data shown here are from the C54 set and at $|\mathbf{p}'|^2 = 4 \cdot (2\pi/L)^2$. As explained in Ref. [23], at each value of $|\mathbf{p}'|^2$, the fit is performed simultaneously for the six data sets.

with the choice of fit range for Eq. (17). To estimate this systematic uncertainty, we calculated the changes in the fitted $F_\pm^{i,n}$ when excluding the data points with the shortest source-sink separation [23]. These changes fluctuate as a function of the momentum, and here we conservatively took the maximum of the change over all momenta as the systematic uncertainty for each data set. In Tables IV and V, we additionally list the corresponding results for $F_1^{i,n} = (F_+^{i,n} + F_-^{i,n})/2$ and $F_2^{i,n} = (F_+^{i,n} - F_-^{i,n})/2$, where the uncertainties take into account the correlations between $F_+^{i,n}$ and $F_-^{i,n}$.

$ \mathbf{p}' ^2/(2\pi/L)^2$	F_+^{C14}	F_+^{C24}	F_+^{C54}	F_+^{F23}	F_+^{F43}	F_+^{F63}
0	1.148(53)	1.126(39)	1.119(39)	1.125(74)	1.117(52)	1.069(62)
1	1.030(50)	1.026(37)	1.023(38)	1.037(68)	1.027(48)	0.993(61)
2	0.926(51)	0.923(38)	0.924(38)	0.922(67)	0.921(47)	0.892(64)
3	0.828(53)	0.843(39)	0.842(39)	0.843(69)	0.845(48)	0.814(64)
4	0.776(51)	0.775(38)	0.772(39)	0.795(70)	0.792(49)	0.761(63)
5	0.693(51)	0.719(38)	0.716(39)	0.754(70)	0.747(50)	0.710(63)
6	0.648(52)	0.673(39)	0.664(39)	0.702(72)	0.700(51)	0.673(64)
8	0.578(56)	0.606(41)	0.610(40)	0.632(75)	0.621(55)	0.624(65)
9	0.549(60)	0.568(45)	0.573(42)	0.604(77)	0.590(59)	0.605(67)

TABLE II. Lattice results for the form factor F_+ .

$ \mathbf{p}' ^2/(2\pi/L)^2$	F_-^{C14}	F_-^{C24}	F_-^{C54}	F_-^{F23}	F_-^{F43}	F_-^{F63}
1	1.80(12)	1.861(98)	1.874(66)	1.70(18)	1.709(93)	1.755(99)
2	1.60(11)	1.615(91)	1.625(63)	1.52(17)	1.540(89)	1.541(98)
3	1.46(12)	1.502(10)	1.513(71)	1.48(18)	1.433(90)	1.415(99)
4	1.17(11)	1.181(85)	1.265(62)	1.29(17)	1.281(89)	1.270(96)
5	1.07(10)	1.110(86)	1.169(63)	1.15(17)	1.177(88)	1.179(95)
6	1.00(11)	1.046(87)	1.101(65)	1.02(17)	1.079(88)	1.115(96)
8	0.82(11)	0.878(88)	0.915(65)	0.89(18)	0.955(90)	0.965(97)
9	0.80(11)	0.814(90)	0.863(69)	0.84(17)	0.93(10)	0.94(10)

TABLE III. Lattice results for the form factor F_- .

$ \mathbf{p}' ^2/(2\pi/L)^2$	F_1^{C14}	F_1^{C24}	F_1^{C54}	F_1^{F23}	F_1^{F43}	F_1^{F63}
1	1.417(64)	1.444(56)	1.448(41)	1.368(98)	1.368(47)	1.374(67)
2	1.263(61)	1.269(53)	1.274(41)	1.220(90)	1.231(43)	1.216(69)
3	1.144(62)	1.172(58)	1.177(44)	1.160(92)	1.139(44)	1.115(69)
4	0.975(56)	0.978(50)	1.018(39)	1.041(90)	1.037(43)	1.016(68)
5	0.879(55)	0.914(50)	0.942(40)	0.951(89)	0.962(42)	0.944(67)
6	0.824(56)	0.860(51)	0.883(41)	0.861(91)	0.890(43)	0.894(67)
8	0.699(59)	0.742(51)	0.763(40)	0.760(95)	0.788(46)	0.795(68)
9	0.672(63)	0.691(52)	0.718(41)	0.722(96)	0.760(52)	0.770(71)

TABLE IV. Lattice results for the form factor F_1 .

$ \mathbf{p}' ^2/(2\pi/L)^2$	F_2^{C14}	F_2^{C24}	F_2^{C54}	F_2^{F23}	F_2^{F43}	F_2^{F63}
1	-0.387(60)	-0.418(43)	-0.425(29)	-0.332(86)	-0.341(47)	-0.381(37)
2	-0.337(56)	-0.346(38)	-0.350(27)	-0.297(82)	-0.309(46)	-0.325(34)
3	-0.316(59)	-0.330(44)	-0.335(31)	-0.317(86)	-0.294(48)	-0.300(35)
4	-0.199(54)	-0.203(36)	-0.247(27)	-0.247(85)	-0.245(48)	-0.254(34)
5	-0.186(54)	-0.196(37)	-0.226(28)	-0.197(82)	-0.215(48)	-0.235(34)
6	-0.176(55)	-0.187(37)	-0.219(29)	-0.159(82)	-0.190(48)	-0.221(35)
8	-0.121(57)	-0.136(41)	-0.153(31)	-0.128(85)	-0.167(50)	-0.171(36)
9	-0.124(60)	-0.123(43)	-0.145(35)	-0.117(82)	-0.170(59)	-0.165(39)

TABLE V. Lattice results for the form factor F_2 .

III. FITS OF THE FORM FACTORS AS FUNCTIONS OF $E_N - m_N$, $m_{u,d}$, AND a

In this section we present fits that smoothly interpolate the E_N -dependence of our $\Lambda_Q \rightarrow p$ form factor results, including corrections to account for the dependence on the lattice spacing and the light-quark mass. In principle, the form of this dependence can be predicted in a low-energy effective field theory combining heavy-baryon chiral perturbation theory for the proton [33, 34] with heavy-hadron chiral perturbation theory [35, 36] for the Λ_Q . However, there are a number of issues that limit the usefulness of this approach for our work. One limitation is that chiral perturbation theory breaks down for momenta $|\mathbf{p}'|$ comparable to or larger than the chiral symmetry breaking scale. Another limitation is that the effective theory also needs to include the Σ_Q and Δ baryons in the chiral loops, which is expected to lead to additional unknown low-energy constants associated with the matching of the $Q \rightarrow u$ current to the $\Sigma_Q \rightarrow p$, $\Lambda_Q \rightarrow \Delta$, and $\Sigma_Q \rightarrow \Delta$ currents in the effective theory. Finally, some of the data sets used here are partially quenched (with valence-quark masses lighter than the sea-quark masses), which further increases the complexity of the effective theory. As in Ref. [23], we therefore use a simple model that successfully describes the dependence of the form factors on E_N , $m_{u,d}$, and a , at the present level of uncertainty. It is given by

$$F_{\pm}^{i,n} = \frac{Y_{\pm}}{(X_{\pm}^i + E_N^{i,n} - m_N^i)^2} \cdot [1 + d_{\pm}(a^i E_N^{i,n})^2], \quad (18)$$

where the position of the pole depends on the pion mass,

$$X_{\pm}^i = X_{\pm} + c_{\pm} \cdot [(m_{\pi}^i)^2 - (m_{\pi}^{\text{phys}})^2], \quad (19)$$

and the term $[1 + d_{\pm}(a^i E_N^{i,n})^2]$ models the lattice discretization artifacts, which are assumed to increase with the proton energy. As discussed above, we calculate the proton energies using the relativistic dispersion relation $E_N^{i,n} = \sqrt{(m_N^i)^2 + n \cdot (2\pi/L)^2}$, where m_N^i is the lattice proton mass for the data set i . The free fit parameters in Eq. (18) are Y_{\pm} , X_{\pm} , d_{\pm} , and c_{\pm} . Note that here we do not include dependence on the strange-quark mass, because none of the hadrons involved contain a valence strange quark. The fits of $F_{\pm}^{i,n}$ using Eq. (18) are shown in Fig. 2, and give the results listed in Table VI. We have also performed independent fits of the data for $F_1^{i,n} = (F_+^{i,n} + F_-^{i,n})/2$ and $F_2^{i,n} = (F_+^{i,n} - F_-^{i,n})/2$, using the functions

$$F_{1,2}^{i,n} = \frac{Y_{1,2}}{(X_{1,2}^i + E_N^{i,n} - m_N^i)^2} \cdot [1 + d_{1,2}(a^i E_N^{i,n})^2], \quad (20)$$

with $X_{1,2}^i = X_{1,2} + c_{1,2} \cdot [(m_{\pi}^i)^2 - (m_{\pi}^{\text{phys}})^2]$. These fits are shown in Fig. 3, and the resulting values of the parameters are given in Table VII.

By construction, Eqs. (18) and (20) reduce to

$$F_{\pm} = \frac{Y_{\pm}}{(X_{\pm} + E_N - m_N)^2}, \quad (21)$$

$$F_{1,2} = \frac{Y_{1,2}}{(X_{1,2} + E_N - m_N)^2} \quad (22)$$

in the continuum limit and at the physical pion mass. These functions are shown at the bottom of Figs. 2 and 3. In the range of $E_N - m_N$ considered here, the numerical results for Eqs. (21) and (22) are consistent with the relations $F_+ = F_1 + F_2$ and $F_- = F_1 - F_2$ within the statistical uncertainties, as expected. In the plots at the bottom of Figs. 2 and 3, the statistical/fitting uncertainty is indicated using the inner error bands. The outer error bands additionally

Parameter	Result
Y_+	$3.24 \pm 0.62 \text{ GeV}^2$
X_+	$1.66 \pm 0.15 \text{ GeV}$
Y_-	$2.92 \pm 0.62 \text{ GeV}^2$
X_-	$1.19 \pm 0.13 \text{ GeV}$

TABLE VI. Results for the form factor normalization and shape parameters Y_{\pm} and X_{\pm} from fits of the lattice QCD results for $F_{\pm}^{i,n}$, using Eq. (18). The covariances of the parameters needed in Eq. (21) are $\text{Cov}(Y_+, X_+) = 0.090 \text{ GeV}^3$ and $\text{Cov}(Y_-, X_-) = 0.080 \text{ GeV}^3$. The results for the parameters describing the quark mass and lattice spacing dependence are $c_+ = 0.38(35) \text{ GeV}^{-1}$, $d_+ = -0.031(81)$, $c_- = -0.22(35) \text{ GeV}^{-1}$, and $d_- = -0.025(94)$.

Parameter	Result
Y_1	$2.97 \pm 0.50 \text{ GeV}^2$
X_1	$1.36 \pm 0.12 \text{ GeV}$
Y_2	$-0.28 \pm 0.11 \text{ GeV}^2$
X_2	$0.81 \pm 0.17 \text{ GeV}$

TABLE VII. Results for the form factor normalization and shape parameters $Y_{1,2}$ and $X_{1,2}$ from fits of the lattice QCD results for $F_{1,2}^{i,n}$, using Eq. (20). The covariances of the parameters needed in Eq. (22) are $\text{Cov}(Y_1, X_1) = 0.057 \text{ GeV}^3$ and $\text{Cov}(Y_2, X_2) = -0.018 \text{ GeV}^3$. The results for the parameters describing the quark mass and lattice spacing dependence are $d_1 = -0.038(70)$, $c_1 = -0.04(30) \text{ GeV}^{-1}$, $d_2 = 0.05(22)$, and $c_2 = -0.53(54) \text{ GeV}^{-1}$.

include estimates of the total systematic uncertainty, arising from the following sources: the matching of the lattice HQET to continuum HQET current, the finite lattice volume, the unphysical light-quark masses, and the non-zero lattice spacing. We discuss these uncertainties below.

As explained in Sec. II, the lattice HQET to continuum HQET matching is performed using one-loop perturbation theory at the scale $\mu = a^{-1}$, followed by a two-loop renormalization-group evolution from $\mu = a^{-1}$ to the scale of the b -quark mass. To estimate the uncertainty resulting from this use of perturbation theory, we vary the scale from $\mu = a^{-1}$ to $\mu = 2a^{-1}$. For the $\Lambda_Q \rightarrow p$ form factors, this results in a change by 7% at the coarse lattice spacing, and 6% at the fine lattice spacing (these relative changes are approximately the same as for $\Lambda_Q \rightarrow \Lambda$ [23]; any difference in the size of the effect has to come from the $\mathcal{O}(a)$ -improvement terms, but their contribution is small). Thus, we take the matching uncertainty for the continuum-extrapolated form factors to be 6%. Finite-volume effects are also estimated in the same way as in Ref. [23]; based on the values of $\exp(-m_\pi L)$ for each data set we estimate the finite-volume effects in the extrapolated form factors to be of order 3%. The extrapolations to the physical pion mass and the continuum limit using our simple fit models (18) and (20) with a small number of parameters cannot be expected to completely remove the errors associated with the unphysical light-quark masses and nonzero lattice spacing. As discussed above, we did not use chiral perturbation theory, and we ignored the fact that some of our lattice results are partially quenched. Similarly, our fit models assume a particular E_N -dependence of the lattice-spacing errors, which was not derived from effective field theory. Following Ref. [23], we estimate the resulting systematic uncertainties by comparing the form factor results from our standard fits to those from fits with the parameters c_\pm , $c_{1,2}$ or d_\pm , $d_{1,2}$ set to zero. In the energy range $0 \leq E_N - m_N \leq 0.7 \text{ GeV}$, the maximum changes when setting $c_\pm = 0$, $c_{1,2} = 0$ are 3% for F_+ , 3% for F_- , 1% for F_1 , and 13% for F_2 . In the same range, the maximum changes when setting $d_\pm = 0$, $d_{1,2} = 0$ are 2% for F_+ , 2% for F_- , 3% for F_1 , and 4% for F_2 . None of these changes are statistically significant; nevertheless we add these percentages in quadrature to the uncertainties from the current matching and from the finite-volume effects.

In summary, we obtain the following estimates of the total systematic uncertainties (valid for $0 \leq E_N - m_N \leq 0.7 \text{ GeV}$):

$$F_+ : \quad \sqrt{(6\%)^2 + (3\%)^2 + (3\%)^2 + (2\%)^2} \approx 8\%, \quad (23)$$

$$F_- : \quad \sqrt{(6\%)^2 + (3\%)^2 + (3\%)^2 + (2\%)^2} \approx 8\%, \quad (24)$$

$$F_1 : \quad \sqrt{(6\%)^2 + (3\%)^2 + (1\%)^2 + (3\%)^2} \approx 7\%, \quad (25)$$

$$F_2 : \quad \sqrt{(6\%)^2 + (3\%)^2 + (13\%)^2 + (4\%)^2} \approx 15\%. \quad (26)$$

Note that in contrast to Ref. [23], here we choose to only evaluate the form factors in the energy region where we have lattice data, and Eqs. (18) and (20) interpolate this data in $E_N - m_N$. While we have investigated extrapolations into the large-energy region, such extrapolations necessarily introduce model dependence (similar to that seen in Ref. [23]) and will not aid in a precision extraction of $|V_{ub}|$ from experiment.

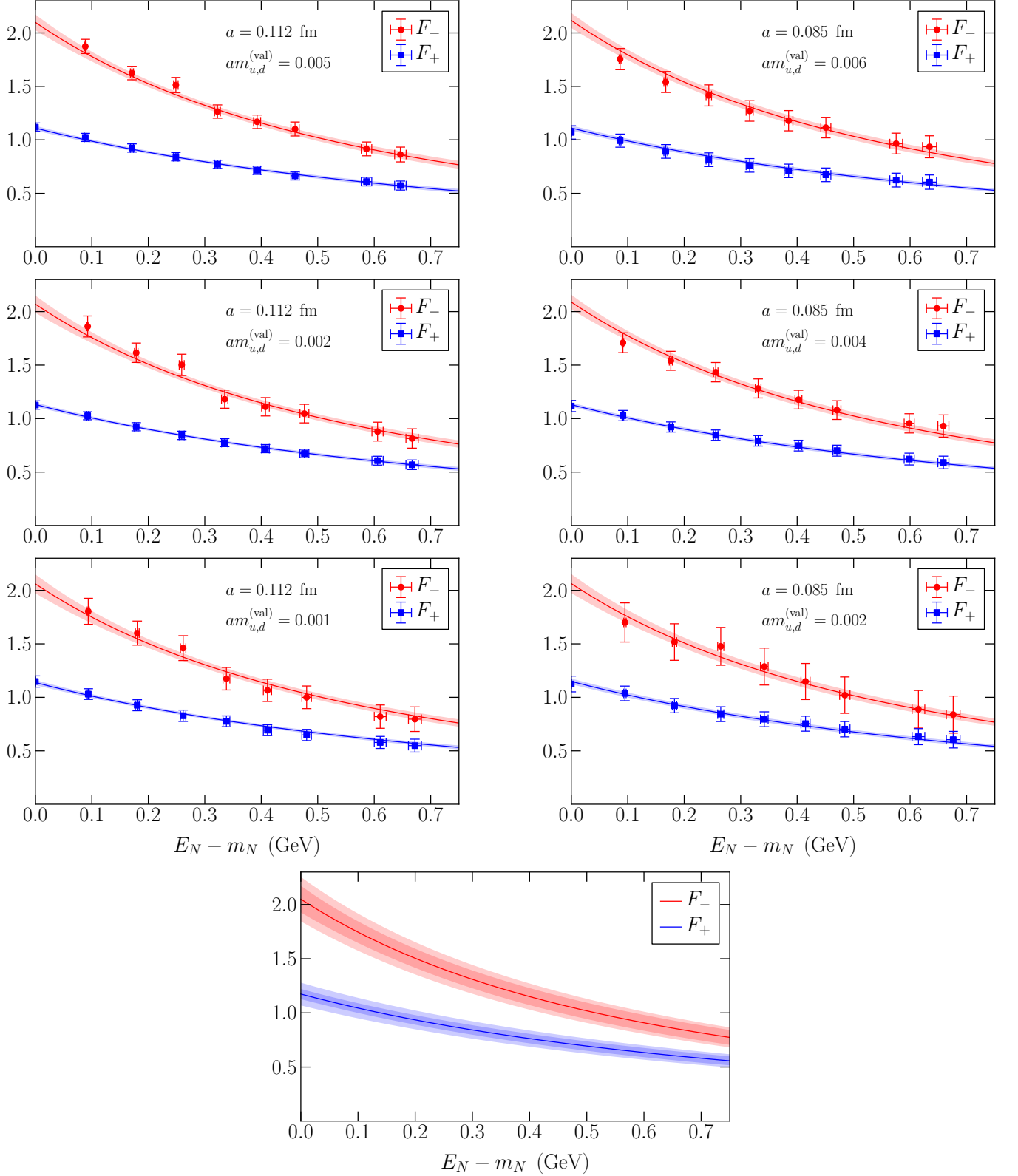


FIG. 2. Fits of the form factor data for F_+ and F_- using Eq. (18). In the upper six plots, we show the lattice results together with the fitted functions evaluated at the corresponding values of the pion mass and lattice spacing. In the lower plot, we show the fitted functions evaluated at the physical pion mass and in the continuum limit. There, the inner shaded bands indicate the statistical/fitting uncertainty, and the outer shaded bands additionally include the estimates of the systematic uncertainty given in Eqs. (23) and (24).

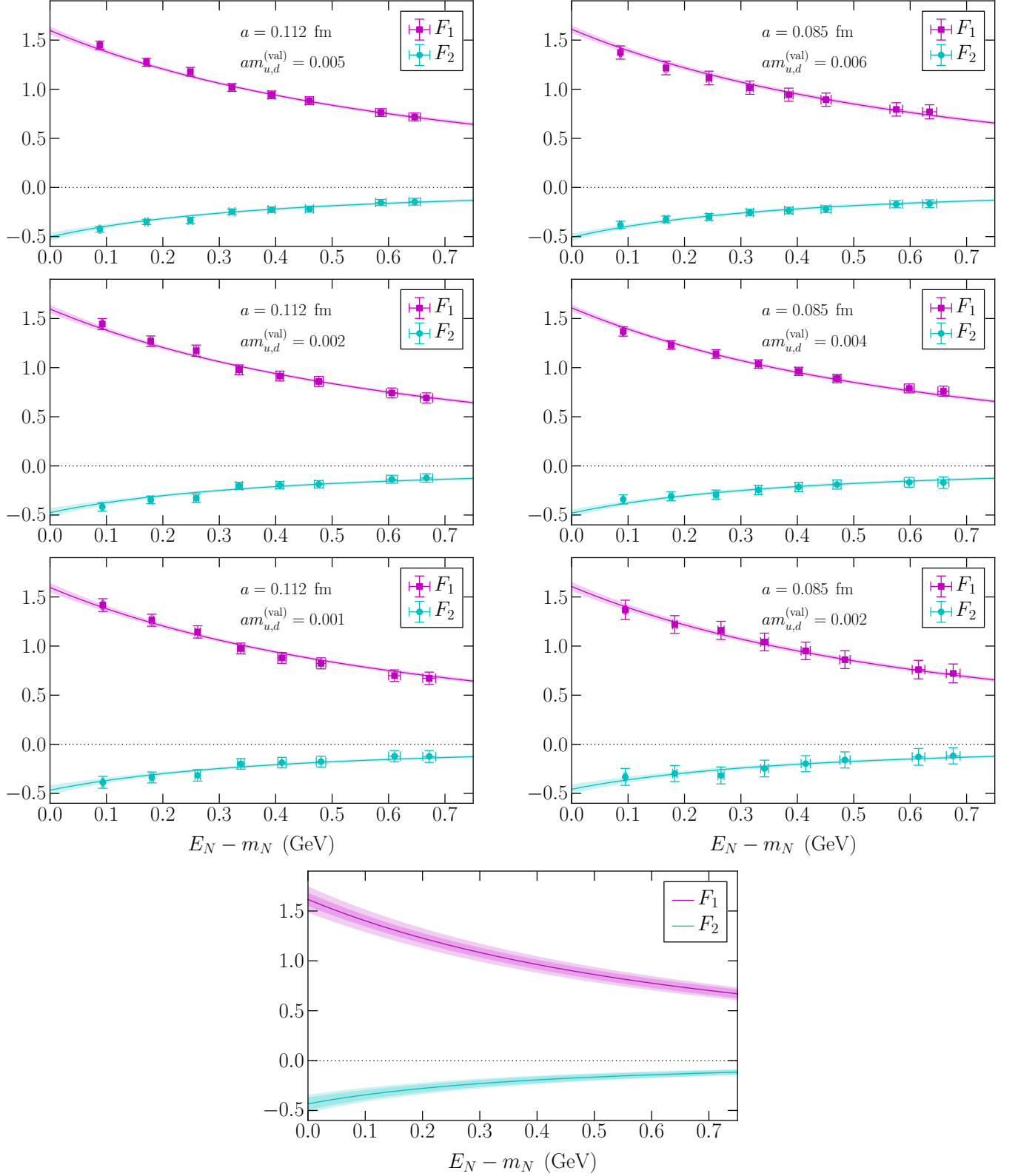


FIG. 3. Fits of the form factor data for F_1 and F_2 using Eq. (20). In the upper six plots, we show the lattice results together with the fitted functions evaluated at the corresponding values of the pion mass and lattice spacing. In the lower plot, we show the fitted functions evaluated at the physical pion mass and in the continuum limit. There, the inner shaded bands indicate the statistical/fitting uncertainty, and the outer shaded bands additionally include the estimates of the systematic uncertainty given in Eqs. (25) and (26).

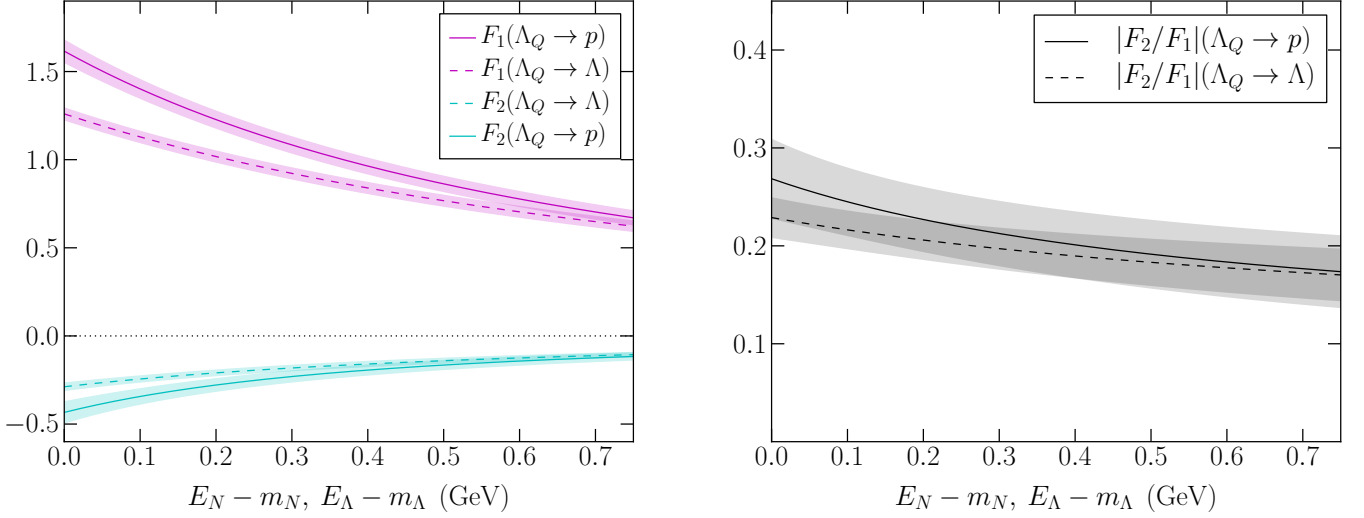


FIG. 4. Left: comparison of the form factors F_1 and F_2 for the $\Lambda_Q \rightarrow p$ transition to the analogous form factors for the $\Lambda_Q \rightarrow \Lambda$ transition [23], all calculated using the same actions and parameters in lattice QCD. Right: comparison of the ratio $|F_2/F_1|$. Only the statistical error bands are shown here for clarity.

IV. COMPARISON WITH OTHER FORM FACTOR RESULTS

It is interesting to compare our results for the $\Lambda_Q \rightarrow p$ form factors to the corresponding results for the $\Lambda_Q \rightarrow \Lambda$ transition obtained in Ref. [23]. This comparison is shown for F_1 and F_2 in Fig. 4, where we plot the form factors vs. $E_N - m_N$ and $E_\Lambda - m_\Lambda$ as before. This choice of variables on the horizontal axis ensures that the points of zero spatial momentum of the final-state hadron (in the Λ_Q rest frame) coincide. As can be seen in the figure, when compared in this way, the $\Lambda_Q \rightarrow p$ form factors have a larger magnitude than the $\Lambda_Q \rightarrow \Lambda$ form factors. This difference is statistically most significant at zero recoil, and becomes less well resolved at higher energy, where our relative uncertainties grow. For the ratio F_2/F_1 , we are unable to resolve any difference between $\Lambda_Q \rightarrow p$ and $\Lambda_Q \rightarrow \Lambda$, as shown on the right-hand side of Fig. 4.

It is also interesting to compare our QCD calculation of the $\Lambda_Q \rightarrow p$ form factors with calculations using sum rules [14, 15] or light-cone sum rules [16–19]. However, most of these studies worked with the relativistic form factors, and focused on the region of high proton momentum (low q^2), where our results would involve extrapolation and hence model dependence. Only Ref. [14] explicitly includes results for the HQET form factors F_1 and F_2 in an energy region that overlaps with the region where we have lattice data. For example, at $E_N - m_N = 0.7$ GeV, the results obtained in Ref. [14] for three different values of the Borel parameter used in that work are $F_1 \approx (0.46, 0.47, 0.50)$ and $F_2 \approx (-0.13, -0.18, -0.27)$, while our lattice QCD calculation gives

$$F_1(E_N - m_N = 0.7 \text{ GeV}) = 0.703 \pm 0.045 \pm 0.049, \quad (27)$$

$$F_2(E_N - m_N = 0.7 \text{ GeV}) = -0.124 \pm 0.025 \pm 0.019, \quad (28)$$

where the first uncertainty is statistical and the second uncertainty is systematic.

V. THE DECAY $\Lambda_b \rightarrow p \ell^- \bar{\nu}_\ell$

In this section, we use the form factors determined above to calculate the differential decay rates of $\Lambda_b \rightarrow p \ell^- \bar{\nu}_\ell$ with $\ell = e, \mu, \tau$ in the Standard Model. The effective weak Hamiltonian for $b \rightarrow u \ell^- \bar{\nu}_\ell$ transitions is

$$\mathcal{H}_{\text{eff}} = \frac{G_F}{\sqrt{2}} V_{ub} \bar{u} \gamma_\mu (1 - \gamma_5) b \bar{\ell} \gamma^\mu (1 - \gamma_5) \nu, \quad (29)$$

with the Fermi constant G_F and the CKM matrix element V_{ub} [37–39]. Higher-order electroweak corrections are neglected. The resulting amplitude for the decay $\Lambda_b \rightarrow p \ell^- \bar{\nu}_\ell$ can be written as

$$\begin{aligned}\mathcal{M} &= -i \langle N^+(p', s') | \ell^-(p_-, s_-) \bar{\nu}(p_+, s_+) | \mathcal{H}_{\text{eff}} | \Lambda_b(p, s) \rangle \\ &= -i \frac{G_F}{\sqrt{2}} V_{ub} A_\mu \bar{u}_\ell(p_-, s_-) \gamma^\mu (1 - \gamma_5) v_{\bar{\nu}}(p_+, s_+),\end{aligned}\quad (30)$$

where A_μ is the hadronic matrix element

$$A_\mu = \langle N^+(p', s') | \bar{u} \gamma_\mu (1 - \gamma_5) b | \Lambda_b(p, s) \rangle. \quad (31)$$

Because we have computed the form factors in HQET, we need to match the QCD current $\bar{u} \gamma_\mu (1 - \gamma_5) b$ in Eq. (31) to the effective theory. This gives (at leading order in $1/m_b$)

$$A_\mu = \sqrt{m_{\Lambda_b}} \langle N^+(p', s') | (c_\gamma \bar{u} \gamma_\mu Q + c_v \bar{u} v_\mu Q - c_\gamma \bar{u} \gamma_\mu \gamma_5 Q + c_v \bar{u} v_\mu \gamma_5 Q) | \Lambda_Q(v, s) \rangle, \quad (32)$$

where Q is the static heavy-quark field, and to one loop, the matching coefficients are given by [40]

$$c_\gamma = 1 - \frac{\alpha_s(\mu)}{\pi} \left[\frac{4}{3} + \ln \left(\frac{\mu}{m_b} \right) \right], \quad (33)$$

$$c_v = \frac{2}{3} \frac{\alpha_s(\mu)}{\pi}. \quad (34)$$

Here we set $\mu = m_b$. We can now use Eq. (3) to express the matrix element A_μ in terms of the form factors F_1 and F_2 :

$$A_\mu = \bar{u}_N(p', s') \left(F_1 + \not{p} F_2 \right) \left(c_\gamma \gamma_\mu + c_v v_\mu - c_\gamma \gamma_\mu \gamma_5 + c_v v_\mu \gamma_5 \right) \sqrt{m_{\Lambda_b}} u_{\Lambda_Q}(v, s). \quad (35)$$

The factor of $\sqrt{m_{\Lambda_b}}$ in Eqs. (32) and (35) results from the HQET convention for the normalization of the state $|\Lambda_Q(v, s)\rangle$ and the spinor $u_{\Lambda_Q}(v, s)$. We can make the replacement $\sqrt{m_{\Lambda_b}} u_{\Lambda_Q}(v, s) = u_{\Lambda_b}(p, s)$, where $p = m_{\Lambda_b} v$, and the spinor $u_{\Lambda_b}(p, s)$ has the standard relativistic normalization. A straightforward calculation then gives the following differential decay rate,

$$\begin{aligned}\frac{d\Gamma}{dq^2} &= \frac{|V_{ub}|^2 G_F^2}{768 \pi^3 q^6 m_{\Lambda_b}^5} (q^2 - m_\ell^2)^2 \sqrt{((m_{\Lambda_b} + m_N)^2 - q^2)((m_{\Lambda_b} - m_N)^2 - q^2)} \\ &\times \left[(4c_\gamma^2 + 4c_\gamma c_v + 2c_v^2) m_\ell^2 \mathcal{F} \mathcal{I} + \left(2c_\gamma^2 (\mathcal{I} + 3q^2 m_{\Lambda_b}^2) + c_v (2c_\gamma + c_v) (\mathcal{I} - 3q^2 m_{\Lambda_b}^2) \right) q^2 \mathcal{F} + 4c_\gamma (c_\gamma + c_v) \mathcal{K} \right],\end{aligned}\quad (36)$$

where we have defined the combinations

$$\mathcal{F} = ((m_{\Lambda_b} + m_N)^2 - q^2) F_+^2 + ((m_{\Lambda_b} - m_N)^2 - q^2) F_-^2, \quad (37)$$

$$\mathcal{I} = m_{\Lambda_b}^4 - 2m_N^2 (m_{\Lambda_b}^2 + q^2) + q^2 m_{\Lambda_b}^2 + m_N^4 + q^4, \quad (38)$$

$$\mathcal{K} = (2m_\ell^2 + q^2)((m_{\Lambda_b} + m_N)^2 - q^2)((m_{\Lambda_b} - m_N)^2 - q^2)(m_{\Lambda_b}^2 - m_N^2 + q^2) F_+ F_-, \quad (39)$$

and, as before, $F_\pm = F_1 \pm F_2$. To evaluate this, we use F_+ and F_- from the fits to our lattice QCD results, which are parametrized by Eq. (18) with the parameters in Table VI. At a given value of q^2 , we evaluate the form factors at

$$E_N - m_N = p' \cdot v - m_N = \frac{m_{\Lambda_b}^2 + m_N^2 - q^2}{2m_{\Lambda_b}} - m_N, \quad (40)$$

with the physical values of the baryon masses (which we take from Ref. [4]).

In Fig. 5, we show plots of $|V_{ub}|^{-2} d\Gamma/dq^2$ for the decays $\Lambda_b \rightarrow p \mu^- \bar{\nu}_\mu$ and $\Lambda_b \rightarrow p \tau^- \bar{\nu}_\tau$ in the kinematic range where we have lattice QCD results (in this range, the results for the electron final state look identical to the results for the muon final state and are therefore not shown). The inner error bands in Fig. 5 originate from the total uncertainty (statistical plus systematic) in the form factors F_+ and F_- . The use of leading-order HQET for the b -quark introduces an additional systematic uncertainty in the differential decay rate, which is included in the outer error band in Fig. 5. At zero hadronic recoil, this uncertainty is expected to be of order Λ_{QCD}/m_b . At non-zero hadronic recoil, one further expects an uncertainty of order $|\mathbf{p}'|/m_b$, because the proton momentum constitutes a new relevant scale. We add

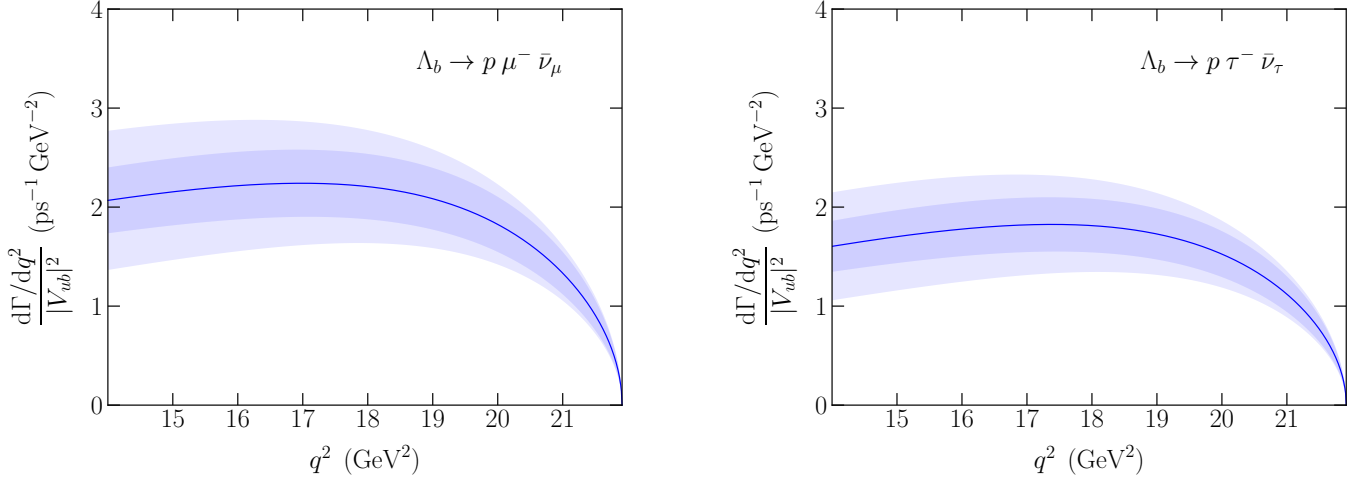


FIG. 5. Our predictions for the differential decay rates of $\Lambda_b \rightarrow p \mu^- \bar{\nu}_\mu$ (left) and $\Lambda_b \rightarrow p \tau^- \bar{\nu}_\tau$ (right), divided by $|V_{ub}|^2$. We only show the kinematic region where we have lattice QCD results for the form factors F_+ and F_- . The inner error band originates from the statistical plus systematic uncertainty in F_\pm . The outer error band additionally includes an estimate of the uncertainty caused by the use of leading-order HQET for the b quark. The plot for $\Lambda_b \rightarrow p e^- \bar{\nu}_e$ is indistinguishable from $\Lambda_b \rightarrow p \mu^- \bar{\nu}_\mu$ and is therefore not shown.

these two uncertainties in quadrature, and hence estimate the systematic uncertainty in $|V_{ub}|^{-2} d\Gamma/dq^2$ that is caused by the use of leading-order HQET to be

$$\sqrt{\frac{\Lambda_{\text{QCD}}^2}{m_b^2} + \frac{|\mathbf{p}'|^2}{m_b^2}}, \quad (41)$$

where we take $\Lambda_{\text{QCD}} = 500$ MeV.

We also provide the following results for the integrated decay rate in the kinematic range of our lattice calculation, $14 \text{ GeV}^2 \leq q^2 \leq q_{\text{max}}^2$ [where $q_{\text{max}}^2 = (m_{\Lambda_b} - m_N)^2$],

$$\frac{1}{|V_{ub}|^2} \int_{14 \text{ GeV}^2}^{q_{\text{max}}^2} \frac{d\Gamma(\Lambda_b \rightarrow p \ell^- \bar{\nu}_\ell)}{dq^2} dq^2 = \begin{cases} 15.3 \pm 2.4 \pm 3.4 \text{ ps}^{-1} & \text{for } \ell = e, \\ 15.3 \pm 2.4 \pm 3.4 \text{ ps}^{-1} & \text{for } \ell = \mu, \\ 12.5 \pm 1.9 \pm 2.7 \text{ ps}^{-1} & \text{for } \ell = \tau. \end{cases} \quad (42)$$

Here, the first uncertainty originates from the form factors, and the second uncertainty originates from the use of the static approximation for the b -quark. With future experimental data, Eq. (42) can be used to determine $|V_{ub}|$.

VI. DISCUSSION

We have obtained precise lattice QCD results for the $\Lambda_Q \rightarrow p$ form factors defined in the heavy-quark limit. These results are valuable in their own right, as they can be compared to model-dependent studies performed in the same limit, and eventually to future lattice QCD calculations at the physical b quark mass. For the $\Lambda_b \rightarrow p \ell^- \bar{\nu}_\ell$ differential decay rate, the static approximation introduces a systematic uncertainty that is of order $\Lambda_{\text{QCD}}/m_b \sim 10\%$ at zero recoil and grows as the momentum of the proton in the Λ_b rest frame is increased. The total uncertainty for the integral of the differential decay rate from $q^2 = 14 \text{ GeV}^2$ to $q_{\text{max}}^2 = (m_{\Lambda_b} - m_N)^2$, which is the kinematic range where we have lattice data, is about 30%. Using future experimental data, this will allow a novel determination of the CKM matrix element $|V_{ub}|$ with about 15% theoretical uncertainty (the experimental uncertainty will also contribute to the overall extraction). The theoretical uncertainty is already smaller than the difference between the values of $|V_{ub}|$ extracted from inclusive and exclusive B meson decays [Eqs. (1) and (2)], and can be reduced further by performing lattice QCD calculations of the full set of $\Lambda_b \rightarrow p$ form factors at the physical value of the b -quark mass. In such calculations, the b quark can be implemented using for example a Wilson-like action [41–43], lattice nonrelativistic QCD [44], or higher-order lattice HQET [45]. Once the uncertainty from the static approximation is eliminated, other systematic uncertainties need to be reduced. In the present calculation, the second-largest source of systematic

uncertainty is the one-loop matching of the lattice currents to the continuum current; ideally, in future calculations this can be replaced by a nonperturbative method. We expect that after making these improvements, the theoretical uncertainty in the value of $|V_{ub}|$ extracted from $\Lambda_b \rightarrow p \ell^- \bar{\nu}_\ell$ decays will be of order 5%, and comparable to the theoretical uncertainty for the analogous $\bar{B} \rightarrow \pi^+ \ell^- \bar{\nu}_\ell$ decays.

ACKNOWLEDGMENTS

We thank Ulrik Egede for a communication about the possibility of measuring $\Lambda_b \rightarrow p \mu^- \bar{\nu}_\mu$ at LHCb. We thank the RBC and UKQCD collaborations for providing the gauge field configurations. This work has made use of the Chroma software system for lattice QCD [46]. WD and SM are supported by the U.S. Department of Energy under cooperative research agreement Contract Number DE-FG02-94ER40818. WD is also supported by U.S. Department of Energy Outstanding Junior Investigator Award DE-SC000-1784. CJDL is supported by Taiwanese NSC Grant Number 99-2112-M-009-004-MY3, and MW is supported by STFC. Numerical calculations were performed using machines at NICS/XSEDE (supported by National Science Foundation Grant Number OCI-1053575) and at NERSC (supported by U.S. Department of Energy Grant Number DE-AC02-05CH11231).

-
- [1] R. Kowalewski (BaBar Collaboration), PoS FPCP **2010**, 028 (2010).
 - [2] T. Mannel, PoS FPCP **2010**, 029 (2010).
 - [3] M. Antonelli *et al.*, Phys. Rept. **494**, 197 (2010) [arXiv:0907.5386].
 - [4] J. Beringer *et al.* (Particle Data Group Collaboration), Phys. Rev. D **86**, 010001 (2012).
 - [5] J. A. Bailey *et al.*, Phys. Rev. D **79**, 054507 (2009) [arXiv:0811.3640].
 - [6] E. Gulez, A. Gray, M. Wingate, C. T. H. Davies, G. P. Lepage, and J. Shigemitsu, Phys. Rev. D **73** (2006) 074502 [Erratum-ibid. D **75** (2007) 119906] [arXiv:hep-lat/0601021].
 - [7] U. Egede, private communication.
 - [8] F. Hussain, D.-S. Liu, M. Kramer, J. G. Körner, and S. Tawfiq, Nucl. Phys. B **370**, 259 (1992).
 - [9] T. Mannel, W. Roberts, and Z. Ryzak, Nucl. Phys. B **355**, 38 (1991).
 - [10] F. Hussain, J. G. Körner, M. Kramer, and G. Thompson, Z. Phys. C **51**, 321 (1991).
 - [11] T. Feldmann and M. W. Y. Yip, Phys. Rev. D **85**, 014035 (2012) [Erratum-ibid. D **86**, 079901 (2012)] [arXiv:1111.1844].
 - [12] T. Mannel and Y.-M. Wang, JHEP **1112**, 067 (2011) [arXiv:1111.1849].
 - [13] W. Wang, Phys. Lett. B **708**, 119 (2012) [arXiv:1112.0237].
 - [14] C.-S. Huang, C.-F. Qiao, and H.-G. Yan, arXiv:hep-ph/9805452v3.
 - [15] R. S. Marques de Carvalho, F. S. Navarra, M. Nielsen, E. Ferreira, and H. G. Dosch, Phys. Rev. D **60**, 034009 (1999) [arXiv:hep-ph/9903326].
 - [16] M.-Q. Huang and D.-W. Wang, Phys. Rev. D **69**, 094003 (2004) [arXiv:hep-ph/0401094].
 - [17] Y.-M. Wang, Y.-L. Shen, and C.-D. Lü, Phys. Rev. D **80**, 074012 (2009) [arXiv:0907.4008].
 - [18] K. Azizi, M. Bayar, Y. Sarac, and H. Sundu, Phys. Rev. D **80**, 096007 (2009) [arXiv:0908.1758].
 - [19] A. Khodjamirian, C. Klein, T. Mannel, and Y.-M. Wang, JHEP **1109**, 106 (2011) [arXiv:1108.2971].
 - [20] F. Bahr, F. Bernardoni, A. Ramos, H. Simma, R. Sommer, and J. Bulava, PoS LATTICE **2012**, 110 (2012) [arXiv:1210.3478].
 - [21] C. M. Bouchard, G. P. Lepage, C. J. Monahan, H. Na and J. Shigemitsu, PoS LATTICE **2012**, 118 (2012) [arXiv:1210.6992].
 - [22] T. Kawanai, R. S. Van de Water, and O. Witzel, PoS LATTICE **2012**, 109 (2012) [arXiv:1211.0956].
 - [23] W. Detmold, C.-J. D. Lin, S. Meinel, and M. Wingate, Phys. Rev. D **87**, 074502 (2013) [arXiv:1212.4827].
 - [24] D. B. Kaplan, Phys. Lett. B **288**, 342 (1992) [arXiv:hep-lat/9206013].
 - [25] Y. Shamir, Nucl. Phys. B **406**, 90 (1993) [arXiv:hep-lat/9303005].
 - [26] V. Furman and Y. Shamir, Nucl. Phys. B **439**, 54 (1995) [arXiv:hep-lat/9405004].
 - [27] Y. Aoki *et al.* (RBC/UKQCD Collaboration), Phys. Rev. D **83**, 074508 (2011) [arXiv:1011.0892].
 - [28] Y. Iwasaki, Report No. UTHEP-118 (1983).
 - [29] Y. Iwasaki and T. Yoshie, Phys. Lett. B **143**, 449 (1984).
 - [30] E. Eichten and B. R. Hill, Phys. Lett. B **240**, 193 (1990).
 - [31] M. Della Morte, A. Shindler, and R. Sommer, JHEP **0508**, 051 (2005) [arXiv:hep-lat/0506008].
 - [32] T. Ishikawa, Y. Aoki, J. M. Flynn, T. Izubuchi, and O. Lottik, JHEP **1105**, 040 (2011) [arXiv:1101.1072].
 - [33] E. E. Jenkins and A. V. Manohar, UCSD-PTH-91-30, Proceedings of the workshop on Effective Field Theories of the Standard Model, Dobogókő, Hungary, August 1991.
 - [34] E. E. Jenkins and A. V. Manohar, Phys. Lett. B **255**, 558 (1991).
 - [35] T.-M. Yan, H.-Y. Cheng, C.-Y. Cheung, G.-L. Lin, Y. C. Lin, and H.-L. Yu, Phys. Rev. D **46**, 1148 (1992) [Erratum-ibid. D **55**, 5851 (1997)].
 - [36] P. L. Cho, Nucl. Phys. B **396**, 183 (1993) [Erratum-ibid. B **421**, 683 (1994)] [arXiv:hep-ph/9208244].
 - [37] N. Cabibbo, Phys. Rev. Lett. **10**, 531 (1963).

- [38] M. Kobayashi and T. Maskawa, Prog. Theor. Phys. **49**, 652 (1973).
- [39] K. G. Wilson, Phys. Rev. **179**, 1499 (1969).
- [40] E. Eichten and B. R. Hill, Phys. Lett. B **234**, 511 (1990).
- [41] A. X. El-Khadra, A. S. Kronfeld, and P. B. Mackenzie, Phys. Rev. D **55**, 3933 (1997) [arXiv:hep-lat/9604004].
- [42] S. Aoki, Y. Kuramashi, and S.-i. Tominaga, Prog. Theor. Phys. **109**, 383 (2003) [arXiv:hep-lat/0107009].
- [43] N. H. Christ, M. Li, and H.-W. Lin, Phys. Rev. D **76**, 074505 (2007) [arXiv:hep-lat/0608006].
- [44] G. P. Lepage, L. Magnea, C. Nakhleh, U. Magnea, and K. Hornbostel, Phys. Rev. D **46**, 4052 (1992) [arXiv:hep-lat/9205007].
- [45] B. Blossier *et al.* (ALPHA Collaboration), JHEP **1209**, 132 (2012) [arXiv:1203.6516].
- [46] R. G. Edwards and B. Joó, Nucl. Phys. Proc. Suppl. **140**, 832 (2005) [arXiv:hep-lat/0409003].